International Symposium
On Turbulence and Shear Flow
Phenomena (TSFP-8)
August 28 - 30, 2013 Poitiers, France

INVESTIGATION OF THE CONTINUOUS AND DISCRETE ADJOINT IN THE CONTROL OF PLANE JETS

Daniel Marinc and Holger Foysi
Chair of Fluid Mechanics
University of Siegen
Paul-Bonatz-Strasse 9-11
daniel.marinc@uni-siegen.de
holger.foysi@uni-siegen.de

ABSTRACT

A comparison of the optimal control of two- and three-dimensional plane jets using the continuous and discrete adjoint of the instationary Navier-Stokes equations was performed. The control aim was to reduce the sound emission in the near far-field by using a heat source actuation within the transitioning jet shear layers. The fully compressible Navier-Stokes equations were solved using dispersion-relation preserving spatial discretization schemes and a low-dissipation-dispersion Runge-Kutta scheme. The Reynolds number based on the slot diameter was set to 2000 and the Mach number to 0.9. Direct numerical as well as large-eddy simulations in two and three dimensions where performed to estimate the influence of modelling and resolution on the results. The results show a slight advantage of using the discrete adjoint, especially when handling boundary conditions, since the calculation of the gradient of the cost functional is more accurate. It is interesting, too, that the control efficiency reduces with increasing resolution and therefore dimension of the control. Reducing it by applying a selected interpolation in the control area shows an increase in efficiency and sound reduction.

Introduction

Optimal control of flows using the adjoint equations has become a valuable tool in fluid mechanics, with applications ranging from aerodynamic shape optimization (Kuruvila *et al.*, 1994; Giles & Pierce, 2000; Brezillon & Gauger, 2004; Giering *et al.*, 2005; Srinath & Mittal, 2010; Zymaris *et al.*, 2010; Jameson & Ou, 2011) to sound reduction in compressible flows (Joslin *et al.*, 2005; Wei & Freund, 2006; Spagnoli & Airiau, 2008; Freund, 2010; Kim *et al.*, 2010; Rumpfkeil & Zingg, 2010; Marinc & Foysi, 2012). The principal task is to minimize a cost functional or objective (unwanted noise or drag, for example). Differential equation constraints are additionally imposed, which here consist of the primal flow equations. The minimization procedure requires the determination of the gradient of this cost functional (Gunzburger, 2002). Unfortunately, a finite difference approach requires $\mathcal{O}(n)$ solutions of our primal flow equations for n different design variables to obtain the gradient, which is impractical. Optimal control based on the adjoint equations on the other hand is *independent* of the number of design parameters. The adjoint may be calculated using two different routes. One possibility is to derive the adjoint equations analytically based on the problem describing partial differential equations (primal), before discretizing the resulting equations ("first optimize then discretize" (FOD). Alternatively, the primal flow equations are discretized first and these already discretized equations are used to determine the discrete adjoint equations ("first discretize then optimize" (FDO)). Both routes lead to different numerical results which are equal only in the limit of infinitely small grid and time steps. For a further discussion of disadvantages and advantages see Gunzburger (2002). For aeroacoustic sound reduction most authors used the continuous adjoint approach, so far (Joslin *et al.*, 2005; Wei & Freund, 2006; Spagnoli & Airiau, 2008; Freund, 2010; Kim *et al.*, 2010; Marinc & Foysi, 2012), making it possible to adjust or change the discretization or boundary treatment of the adjoined compared to the primal flow equations. However, Marinc & Foysi (2012) showed recently, that the gradient direction deviates from the exact gradient direction towards the end of the control horizon for instationary control simulations (figure 1, normalization was done by the corresponding values at the nozzle exit). It's possible to even have opposite gradient directions rendering the minimization ineffective or even unsuccessful. Among the possible reasons are inconsistencies due to a different discretization of the adjoint compared to the primal flow equations, different boundary conditions, additional numerical filtering for stabilization in critical areas with large gradients or grid resolution. This leads to adjoint equations which deviate from those obtained by a formal derivation using the primal equations, resulting in inconsistent gradients. The discrete adjoint on the other hand exactly corresponds to its discrete primal equations leading to a gradient direction which is accurate even to machine precision. The discussion shows, that a comparison of the discrete and continuous adjoint for

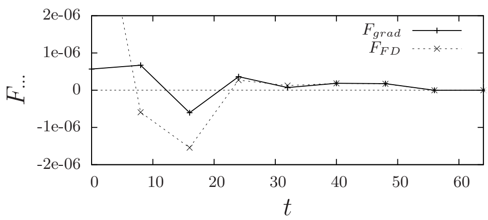

Figure 1. Comparison of the gradient direction of the plane jet using the continuous adjoint (F_{grad}) with that obtained using finite-differences (F_{FD}), from Marinc & Foysi (2012).

Table 1. Parameters of the plane jet simulations. The domain lengths L_i were normalized by the jet diameter D. The Reynolds number is $Re = U_j D/\mu_j = 2000$ and the Mach number is $Ma = U_j/c_j = 0.9$ for all simulations. The number of grid points in the respective coordinate directions are represented by n_i. $\Delta_{i,min}$ gives the minimum grid- spacing in direction i. Δt gives the time step used during the optimization computations non-dimensionalized by D/U_j . The subscript j denotes mean values at the jet inflow.

Case	L_x	L_y	L_z	n_x	n_y	n_z	$\Delta_{x,min}$	$\Delta_{y,min}$	$\Delta_{z,min}$	Δt
DNS2D	30	-	34	512	1	640	0.04	-	0.036	0.017
ELES3D	37	9	28	416	64	320	0.071	0.014	0.065	0.03
LES3D	37	9	28	512	160	400	0.051	0.056	0.051	0.021
DNS3D	37	9	28	800	288	600	0.029	0.031	0.028	0.012

large time dependent minimization problems is of utmost interest in order to identify possible deficiencies and to give guidelines for successful continuous adjoint calculations.

Numerical method

The governing equations are the compressible Navier-Stokes-equations in one of its usual formulations:

$$\frac{\partial \rho}{\partial t} = \frac{\partial m_i}{\partial x_i} \tag{1}$$

$$\frac{\partial m_i}{\partial t} = -\frac{\partial p}{\partial x_i} - \frac{\partial}{\partial x_j}\rho u_j u_i + \frac{\partial}{\partial x_j}\tau_{ji} \tag{2}$$

$$\frac{\partial p}{\partial t} = -\frac{\partial}{\partial x_i} p u_i + \frac{\partial}{\partial x_i}\lambda(\gamma-1)\frac{\partial}{\partial x_i}T - (\gamma-1)p\frac{\partial}{\partial x_i}u_i + (\gamma-1)\tau_{ij}\frac{\partial}{\partial x_j}u_i \tag{3}$$

where ρ is the density, u_i are the velocities in direction i, γ the ratio of the specific heats, T temperature and λ the heat conductivity. Furthermore we have $m_i = \rho u_i$ and

$$\tau_{ij} = \mu s_{ij} = \mu\left(\frac{\partial u_i}{\partial x_j} + \frac{\partial u_i}{\partial x_j} - \delta_{ij}\frac{2}{3}\frac{\partial u_k}{\partial x_k}\right), \tag{4}$$

where μ is the viscosity.

The equations of motion are solved in cartesian coordinates. To minimize errors in the adjoint optimization a low-dispersion-dissipation fourth-order Runge-Kutta scheme of Hu *et al.* (1996) in its low storage form is applied. Spatial differentiation is performed using optimized explicit DRP-SBP (dispersion-relation-preserving summation by parts) finite-difference operators of sixth-order as in Johansson (2004). The subgrid-scale modeling for the large eddy simulation is performed by using a variant of the approximate deconvolution method originally introduced by Stolz *et al.* (Stolz & Adams, 1999; Stolz *et al.*, 2001), which is based on explicit filtering alone (Mathew *et al.*, 2003, 2006; Foysi *et al.*, 2010). This approach is similar to the selective filtering procedure suggested in Bogey & Bailly (2006). The filter was also applied to remove grid to grid oscillations in the direct numerical simulations.

To allow acoustic waves to pass the boundaries of the numerical domain without reflections, characteristic boundary conditions after Lodato *et al.* (2008) were implemented, together with a combination of grid stretching and spatial filtering within a sponge zone surrounding the physical domain close to the boundaries to damp disturbances (Foysi *et al.*, 2010), as indicated in figure 2.

The resolution and grid size of the two- and three-dimensional DNS as well as LES were chosen based on similar simulations at comparable Reynolds numbers in Foysi *et al.* (2010) and data in Stanley & Sarkar (2000), where grid resolution tests have been performed. Table 1 lists various paramaters including the number of grid points and the domain size of the direct numerical and large-eddy simulations (LES). Most of the flow control cases dealing with sound reduction so far were 2D-simulations, therefore we included a reference case called *DNS2D*, for comparison. Furthermore, two LES with different grid resolutions were performed (a coarse (*ELES3D*) and a well resolved one (*LES3D*)) to test the effect of the dimension of the control and possible influences of the filtering on the optimization. A full three-dimensional optimal control simulation (*DNS3D*) serves for comparison and should provide insight into differences to the 2D case and the LES. Transition to turbulence was triggered by convecting disturbances obtained through separate precursor simulations of plane temporally evolving mixing layers with initially smaller momentum thickness into the shear layers (see Foysi *et al.* (2010) and Marinc & Foysi (2012) for details).

Optimization

In this work we aim to minimize the noise emission of a jet. A measure for the far field sound pressure is given by

$$\mathfrak{J} = \int_\Omega \int_T (p(\mathbf{x},t) - \overline{p}(\mathbf{x}))^2 \, dt \, d\Omega, \tag{5}$$

which serves as our performance index or cost functional. Here T is the control-horizon, Ω is a small volume in the farfield of the jet and $\overline{p}$ denotes the temporal average of the pressure over the interval T. In this work we aim to find control-parameters which minimize $\mathfrak{J}$ under the constraint, that the solution has to fulfill the Navier-Stokes-equations. The control is applied within two regions located in both jet shear layers near the inflow, where heating or cooling is applied (see figure 2). Accordingly, a forcing term $R\rho f g$ is added to the right-hand side (RHS) of the pressure equation, where g is the control, R the ideal gas constant and f is a shape function to prevent discontinuities when transitioning from uncontrolled to controlled areas. In this work, the gradient $\mathscr{G}$ with respect to the control is needed to find the minimum of our cost functional. An efficient way in calculating this gradient is in using the so-called adjoint flow field (Gunzburger (2002)). In our case we get $\mathscr{G}(g) = d\mathfrak{J}/dg = \rho R f p^*$ and used it in an LBFGS (low-storage BFGS) optimization routine (Nocedal & Wright, 2006). A backtracking algorithm with quadratic interpolation or a Wolfe-linesearch (mixed quadratic/cubic interpolation, Nocedal & Wright (2006)) were applied in addition to update the control from the previous iteration, $g^{new} = g^{old} - r\,\mathscr{G}(g^{old})$. Here, r denotes a generalized distance in control space. Various optimization schemes

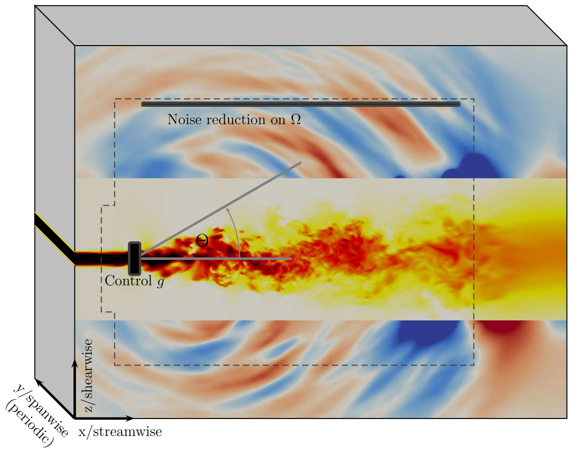

Figure 2. Illustration of the control-setup for the simulations. The jet is heated/cooled in a small volume within the shearlayers of the jet. The noise-reduction is expected to take place in the observer region in the near far-field of the jet, indicated by a thick black horizontal line. Shown is the streamwise velocity component in the turbulent region and the pressure in the farfield. The area outside the dashed lines are unphysical sponge-regions.

were tested, including different variants of conjugate gradient schemes as well as schemes using second-order gradient information (Newton conjugate-gradient, Newton-Lanczos), various line-search methods and trust-region algorithms. The LBFGS together with a Wolfe-linesearch performed best (details are given at the conference). The adjoint pressure p^* which is part of the optimization process is obtained from the *time-dependent* solution of the adjoint Navier-Stokes equations, derived as described in Gunzburger (2002) or Bewley *et al.* (2001). We then get

$$\frac{\partial \rho^*}{\partial t} = u_i u_i^* + T C_V T^* \tag{6}$$

$$\frac{\partial m_i^*}{\partial t} = -\frac{\partial \rho^*}{\partial x_i} - u_j \frac{\partial m_j^*}{\partial x_i} - u_i^* \tag{7}$$

$$\frac{\partial p^*}{\partial t} = -\frac{\partial m_i^*}{\partial x_i} + \frac{\partial u_i^*}{\partial x_i}(\gamma-1)p^* - (\gamma-1)u_i \frac{\partial p^*}{\partial x_i} \tag{8}$$

with

$$\rho u_i^* = m_j \frac{\partial m_i^*}{\partial x_j} + \frac{\partial \tau_{ji}^*}{\partial x_j} - (\gamma-1)\frac{\partial}{\partial x_j}\tau_{ji}p^* + (\gamma-1)p\frac{\partial p^*}{\partial x_i} + \frac{\partial}{\partial x_i}\left(\frac{\partial u_i}{\partial x_i}\right)^* \tag{9}$$

$$\tau_{ij}^* = \mu\left(\frac{\partial m_i^*}{\partial x_j} + \frac{\partial m_j^*}{\partial x_i} - 2(\gamma-1)p^*\left(\frac{\partial u_i}{\partial x_j} + \frac{\partial u_j}{\partial x_i}\right)\right) \tag{10}$$

$$\left(\frac{\partial u_i}{\partial x_i}\right)^* = -\frac{2}{3}\tau_{ii}^* + (\gamma-1)pp^* \tag{11}$$

$$\rho C_V T^* = -s_{ij}\frac{\partial \mu}{\partial T}\frac{\partial m_i^*}{\partial x_j} + \frac{C_P}{Pr}(\gamma-1)\mu\frac{\partial^2 p^*}{\partial {x_i}^2} + s_{ij}(\gamma-1)p^*\frac{\partial \mu}{\partial T}\frac{\partial u_i}{\partial x_j}, \tag{12}$$

where $\cdot^*$ denotes the adjoint quantity of the primal variable. The discrete adjoint is derived, based on the discrete Runge-Kutta sub-step (Φ: vector of state variables)

where F_s is the discrete representation of a filter operator at step s, g_i are $M+1$ control vectors and $\gamma_{s,i}$ are scalars

$$\begin{aligned}
\mathbf{k}_0 &= 0 \\
\mathbf{\Phi}_0 &= \mathbf{\Phi}_{\text{init}} \\
\mathbf{k}_s &= \alpha_{s-1}\mathbf{k}_{s-1} + \Delta t\left(R(\mathbf{\Phi}_{s-1}) + \sum_{i=0}^{M}\gamma_{s-1,i}g_i\right) && s\in\{1\dots N\} \\
\mathbf{\Phi}_s &= F_s\left[\mathbf{\Phi}_{s-1} + \beta_{s-1}\mathbf{k}_s\right] && s\in\{1\dots N\},
\end{aligned} \tag{13}$$

representing the strength of the control g_i at step s. $R(\Phi)$ indicates the right-hand side of the Navier-Stokes equations and the α_s and β_s are parameters given in Hu *et al.* (1996). If the cost functional is given by $\Im = \sum_{s=0}^{N}\Im_s(\Phi_s)$, the Lagrangian is determined to be

$$\begin{aligned}
L = &\sum_{s=0}^{N}\Im_s(\mathbf{\Phi}_s) - \sum_{s=1}^{N}\xi_s^T\left(\mathbf{k}_s - \alpha_{s-1}\mathbf{k}_{s-1} - \Delta t\left(R(\mathbf{\Phi}_{s-1}) + \sum_{i=0}^{M}\gamma_{s-1,i}g_i\right)\right) \\
&- \sum_{s=1}^{N}\omega_s^T\left[\mathbf{\Phi}_s - F_s\left[\mathbf{\Phi}_{s-1} + \beta_{s-1}\mathbf{k}_s\right]\right] - \xi_0^T\mathbf{k}_0 - \omega_0^T\left[\mathbf{\Phi}_0 - \mathbf{\Phi}_{\text{init}}\right]
\end{aligned} \tag{14}$$

with discrete adjoint variables ξ_s, ω_s. A variation of the Lagrangian with respect to the state variables finally gives

$$\begin{aligned}
\frac{\partial L}{\partial \mathbf{\Phi}}\mathbf{\Phi}'_s = &\sum_{s=0}^{N}\left.\frac{\partial \Im_s}{\partial \mathbf{\Phi}}\right|_{\mathbf{\Phi}_s}\mathbf{\Phi}'_s - \sum_{s=1}^{N}\xi_s^T\left(-\Delta t\left.\frac{\partial R}{\partial \mathbf{\Phi}}\right|_{\mathbf{\Phi_{s-1}}}\mathbf{\Phi}'_{s-1}\right) \\
&- \sum_{s=1}^{N}\omega_s^T\left(\mathbf{\Phi}'_s - F_s\mathbf{\Phi}'_{s-1}\right) - \omega_0^T\mathbf{\Phi}'_0
\end{aligned} \tag{15}$$

$$\frac{\partial L}{\partial \mathbf{k}}\mathbf{k}'_s = -\sum_{s=1}^{N}\xi_s^T\left(\mathbf{k}'_s - \alpha_{s-1}\mathbf{k}'_{s-1}\right) - \sum_{s=1}^{N}\omega_s^T\left[-F_s\beta_{s-1}\mathbf{k}'_s\right] - \xi_0^T\mathbf{k}'_0$$

leading to the adjoint Runge-Kutta integration

$$\begin{aligned}
\omega_N &= \left(\left.\frac{\partial \Im_N}{\partial \mathbf{\Phi}}\right|_{\mathbf{\Phi}_N}\right)^T \\
\xi_N &= \beta_{N-1}F_N^T\omega_N \\
\omega_s &= F_{s+1}^T\omega_{s+1} + \Delta t\left(\left.\frac{\partial R}{\partial \mathbf{\Phi}}\right|_{\mathbf{\Phi_s}}\right)^T\xi_{s+1} + \left(\left.\frac{\partial \Im_s}{\partial \mathbf{\Phi}}\right|_{\mathbf{\Phi}_s}\right)^T \\
\xi_s &= \alpha_s\xi_{s+1} + \beta_{s-1}F_s^T\omega_s \\
\xi_0 &= \alpha_0\xi_1
\end{aligned}$$

The index s runs from 0 to $N-1$ for ω and from 1 to $N-1$ for ξ. The boundary condition is given for $s=N$ indicating that the integration is backwards in time. Using these results, the gradient is determined to be

$$\left(\frac{d\Im}{dg_i}\right)^T = \left(\frac{\partial L}{\partial g_i}\right)^T = \Delta t\sum_{s=1}^{N}\gamma_{s-1,i}\xi_s \quad i\in\{0\dots M\}$$

For the continuous adjoint non-reflecting boundary conditions were developed (Marinc & Foysi, 2012). No such derivation is necessary for the discrete adjoint, which is solely determined by the chosen discretization. The continuous and discrete adjoint implementation were validated using the anti-sound test case (Wei & Freund, 2006). Furthermore, for the discrete adjoint sensitivities were compared with sensitivities obtained via complex differentiation. Additionally, the correct transposition was tested using random vectors, showing it to be accurate up to machine precision. The linear response of the cost functional to a perturbation of the control was calculated, too, using the sensitivity equations and the gradient of the Lagrangian.

Results

In a first test the continuous and discrete adjoint were used to minimize the cost functional for case *DNS2D* (figure 3). Both approaches were able to reduce the functional and the sound emmission, the discrete approach, however, performed better leading to a greater reduction in two dimensions. The performance was even better for long control horizons (not shown), indicating that inconsistencies introduced by filtering or the boundary conditions clearly

Table 2. List of the different cases considered for testing of the gradient accuracy for case *LES3D*. RK: formulation used for the RK iteration. RHS: formulation used for the RHS. fsave: number of RK iterations after which the flow field was saved. Save-type: single or double precision. Boundary: boundary treatment details.

Case	RK	RHS	save	save-type	boundary
ContNoBC	continuous	continuous	2	double	non
ContSpng	continuous	continuous	2	double	sponge
ContF2	continuous	continuous	2	double	non-reflecting
ContF4	continuous	continuous	4	double	non-reflecting
ContF8	continuous	continuous	8	double	non-reflecting
ContF16	continuous	continuous	16	double	non-reflecting
Mixed	discrete	continuous	recompute	double	non-reflecting
Ref	discrete	discrete	recompute	double	discrete
DiscF2	discrete	discrete	2	double	discrete
DiscF4	discrete	discrete	4	double	discrete
DiscF8	discrete	discrete	8	double	discrete
DiscF16	discrete	discrete	16	double	discrete

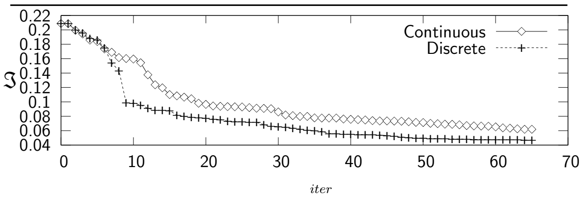

Figure 3. Comparison of the reduction of the cost-function, plotted over the number of LBFGS-iterations for case *DNS2D*.

affect the optimization performance.

For solving the compressible Navier-Stokes equations various boundary conditions are found in the literature, using non-reflecting boundary conditions (see discussion in Colonius (2004)) or sponge regions (Bodony, 2005; Mani, 2012). For the adjoint, too, it is necessary to guarantee disturbances to cross the boundaries unobstracted, otherwise it is possible for reflected waves to interact with the actuator position and instead of controlling the target region the inflow region could be influenced. Additionally, the 2D results indicate that even small changes in the adjoint can have a large effect on the optimization. For this reason different cases were investigated using various combinations of boundary conditions for the continuous adjoint, as tabulated in table 2, for case *LES3D*.

Figure 4 shows the correlation coefficient calculated using the continuous and "exact" adjoint gradient over time for some of these cases. The "exact" gradient was defined to be the full solution of the discrete adjoint optimization problem. As the adjoint equations are solved backwards in time, the correlation is highest at large non-dimensional times and decreases towards the beginning of the time horizon. Using only the mild sponge regions present in the primal flow equations no further boundary treatment was used for the adjoint in case *ContNoBC*, simulated as a reference. In case *ContSpng* a strong sponge region was added to the adjoint equations to damp unwanted disturbances, thereby introducing inconsistencies between primal and adjoint. This approach was motivated by the similar strategy used for the primal flow equations (Bodony, 2005; Mani, 2012). Both simulations are seen to become decorrelated from the exact solution, soon. The sponged solution deviates from that point on, when oblique traveling disturbances reach the inflow boundary of the jet and get, although damped, reflected. Case *ContF2*, on the other hand, uses non-reflecting boundary conditions for the adjoint. Here, the flow fields were stored every second time step for use within the adjoint computation, whereas in case *Mixed* a recomputation of the flow fields within each time interval was performed. Additionally, a mixed calculation approach was used for this case, in that the discrete adjoint Runge-Kutta step was used together with the continuous adjoint for the right-hand-side (RHS). We observe a good agreement of the continuous adjoint gradient with its exact value, when using the characteristic boundary conditions. However, with increasing simulation time deviations occur due to slight inconsistencies introduced by filtering and the boundary conditions, for example. Here, too, the deviations start to increase as soon as the disturbances reach the boundary, nevertheless, the boundary conditions are able to transmit most of them such that large deviations don't build up. No advantage is gained by using a mixed approach, however. The gradient of the discrete adjoint solution is depicted in figure 5. The different curves indicate solutions obtained by using different data storage frequencies of the primal flow solution. This approach was motivated by the large amount of data of the primal equations which needs to be stored to advance the adjoint. Instead of using checkpointing strategies, we used a third-order accurate interpolation scheme to determine the fields at time steps within each time interval. A recomputation of the flow fields was performed for the reference case, with details to be reported elsewhere. A very accurate solution is obtained if the data storage freqency is equal and below 4 (cases *DiscF2, DiscF4*), thereafter, the performance deteriorates. A closer inspection by using the power spectrum of the different flow variables revealed, that increasing parts of the spectrum which don't just correspond to numerical white noise are neglected (not shown). For a data storage frequency of 8, for example, the neglected modes car-

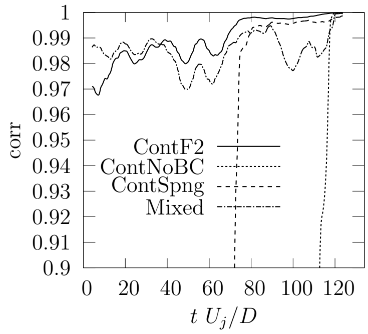

Figure 4. Correlation coefficient of the continuous adjoint gradient with the "exact" gradient for different choices of boundary conditions, for case *LES3D*. As discussed in the text, it is seen that proper adjoint boundary conditions are important.

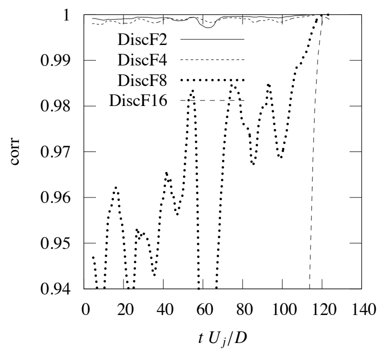

Figure 5. The correlation coefficient of approximations to the discrete adjoint gradient with the "exact" gradient for case *LES3D*. The approximations were obtained by using different data storage frequencies of the primal solution. The number indicates the number of Runge-Kutta time steps after which data storage takes place.

ried less then one percent of the total power, indicating, that an accurate reconstruction of the flow fields is of paramount importance.

For three-dimensional optimization simulations, the performance of the discrete and continuous adjoint is similar, as can be seen in figure 6, for example. Since these optimization methods only converge to local instead of global minima, the initial conditions may determine the subsequent performance. As this case indicates a stronger reduction for the continuous case, the discrete solution was restarted by making use of a flow field obtained from the continuous adjoint optimization ("+"-symbols). As expected, both approaches perform similar then, emphasizing the importance of the choice of the initial condition in obtaining a strong minimum.

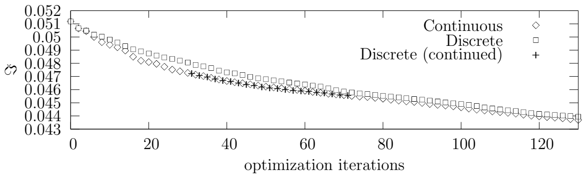

Figure 6. Reduction of the cost-functional as a function of the optimization iterations for case *ELES3D*.

It was recognized, too, that the sound reduction became smaller for the three-dimensional case compared to DNS2D. Two different LES simulation with coarse (*ELES3D*) and fine resolution (*LES3D*) and a DNS were performed because of that, to identify possible modeling errors due to the LES approach. However, by investigating figure 7 we observe a tendency of decreasing performance of the control with increasing resolution and therefore dimension of the control space, due to the fact that the area of application of the control was the same for all cases. The two-dimensional case *DNS2D* has a much smaller control space dimension due to the missing third dimension and the larger time-steps and shows a much stronger cost functional reduction. Additionally, the complexity of the turbulence is reduced, which is revealed in the more coherent structures and is linked to the missing vortex-stretching mechanism. Therefore, a test was performed by updating the control only at every n^{th} grid point in the spatial directions as well as at every δ timesteps and interpolating the control in between using a Catmull-Rom spline (Marschner & Lobb, 1994). As a consequence, it's not further possible to influence the whole spectrum using this type of approach, with the hope of better control efficiency due to a reduction of the control dimension. It is clearly seen in figures 8 and 9, that the cost functional reduction is indeed better when reducing the control space dimension for the LES and DNS. An additional case using only every 5th point and every 8th time step shows no further improvement compared to using every third point and time step. This indicates, that a balance between control space reduction and controllability was reached, here. Nevertheless, a reduction as the one observed for case *DNS2D* is still not reached. The LES performs better than the DNS, however, the effective Reynolds number of the large-eddy simulations is lower due to the increased viscosity as a consequence of the subgrid - modelling.

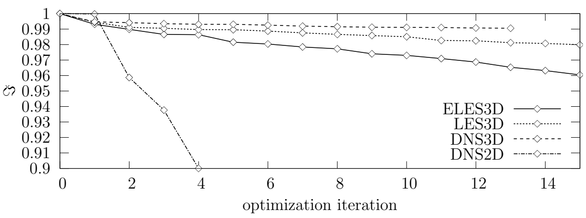

Figure 7. Reduction of the cost-functional normalized with its starting value as a function of the optimization iterations for the discrete adjoint simulations. The reduction clearly decreases with increasing dimension of the control.

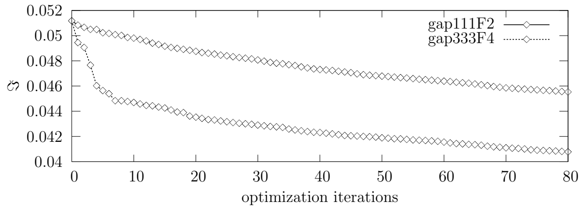

Figure 8. Comparison of the cost functional plotted over the optimization iterations for case *ELES3D*, using two different cases of data reduction. Here, gap$\alpha\beta\gamma$Fδ refers to a simulation using every αth, βth and γth grid point and every δth time step for application of the control.

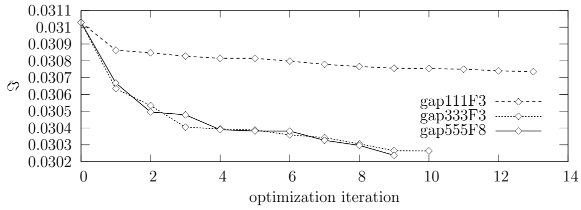

Figure 9. Comparison of the cost functional plotted over the optimization iterations for case *DNS3D*, using different cases of data reduction. For the notation see figure 8.

Conclusion

Adjoint control simulations to reduce the sound emission in the near farfield of plane jets were performed using two- and three-dimensional DNS and LES. The continuous and discrete adjoint equations were derived and used for obtaining the gradient, needed to reduce the cost functional by making use of an LBFGS method with a Wolfe line-search. As the continuous adjoint is subject to inconsistencies due to possible differences in the discretization and boundary conditions of the adjoint equations, which are often treated numerically different from its corresponding primal equations, a comparison between the continuous and discrete adjoint was performed. The discrete adjoint, which is computed up to machine precision, provided the "exact" gradient to compare with. Using various approaches to calculate the boundary conditions for the continuous adjoint, the necessity for non-reflecting boundary conditions (NRBC) together with strong sponge regions for the continuous adjoint became obvious. As the NRBCs only allow waves approaching the boundary normally to be transmitted, reflections of oblique waves occur and lead to sensitivities in this region, resulting in the control trying to influence the boundary. To avoid such problems for the discrete adjoint, a strong sponge for the primal was used to reduce the sensitivities there, the difference in performance of both methods was, however, small. With increasing resolution and therefore an increasing range of scales and control space dimension, a decrease in control efficiency could be observed. A similar observation for channel flow with increasing Reynolds number was found by Collis *et al.* (2000). This increased complexity results in problems, since the gradient based optimization procedures usually don't converge to a global, but local minimum. This could be clearly seen for the performed discrete adjoint optimization using LES, which performed worse in one case than the continous adjoint approach. Furthermore, the increased control dimension with increasing resolution could be indentified, as suspected, to be one reason for the decreased control efficiency. Using only a limited number of points and timesteps for the control field in addition to interpolation in between, the efficiency could be drastically increased. A more detailed investigation will be presented at the conference, nevertheless, the results show that further research is still necessary to identify possibilities to reduce the control dimension and to make use of global optimization procedures.

REFERENCES

Bewley, T., Moin, P. & Teman, R. 2001 DNS-based predictive control of turbulence: an optimal benchmark for feedback algorithms. *J. Fluid Mech.* **447**, 179–225.

Bodony, D.J. 2005 Analysis of sponge zones for computational fluid mechanics. *J. of Comp. Phys.* **212**, 681–702.

Bogey, C. & Bailly, C. 2006 Large eddy simulation of round free jets using explicit filtering with/without dynamic Smagorinsky model. *to appear in Int. J. Heat and Fluid Flow* .

Brezillon, J. & Gauger, N.R. 2004 2d and 3d aerodynamic shape optimisation using the adjoint approach. *Aerospace Science and Technology* **8** (8), 715 – 727.

Collis, S.S., Chang, Y., Kellog, S. & Prabhu, R.D. 2000 Large eddy simulation and turbulence control. *AIAA Paper 2000-2564* .

Colonius, T. 2004 Modeling Artificial Boundary Conditions for Compressibe Flow. *Ann. rev. Fluid. Mech.* **36**, 315–345.

Foysi, H., Mellado, M. & Sarkar, S. 2010 Simulation and comparison of variable density round and plane jets. *International Journal of Heat & Fluid Flow* **31**, 307–314.

Freund, Jonathan B. 2010 Adjoint-based optimization for understanding and suppressing jet noise. *Procedia Engineering* **6**, 54 – 63, iUTAM Symp. on Comput. Aero-Acoustics f. Aircraft Noise Pred.

Giering, R., Kaminski, T. & Slawig, T. 2005 Generating efficient derivative code with taf: Adjoint and tangent linear euler flow around an airfoil. *Future Generation Computer Systems* **21** (8), 1345 – 1355.

Giles, M.B. & Pierce, N.A. 2000 An introduction to the adjoint approach to design. *Flow, Turbulence and Combustion* **65(3-4)**, 393–415.

Gunzburger, Max D. 2002 *Perspectives in Flow Control and Optimization*. Philadelphia, PA, USA: SIAM.

Hu, F.Q., Hussaini, M.Y. & Manthey, J.L. 1996 Low-dissipation and lowdispersion runge-kutta schemes for computational acoustics. *J. Comput. Phys.* **124**, 177–197.

Jameson, Antony & Ou, Kui 2011 50 years of transonic aircraft design. *Progress in Aerospace Sciences* **47(5)**, –.

Johansson, Stefan 2004 High order finite difference operators with the summation by parts property based on DRP schemes. *Tech. Rep.* 2004-036. it.

Joslin, Ronald D., Thomas, Russell H. & Choudhari, Meelan M. 2005 Synergism of flow and noise control technologies. *Progress in Aerospace Sciences* **41** (5), 363 – 417.

Kim, J., Bodony, D.J. & Freund, J.B. 2010 A High-Order, Overset-Mesh Algorithm for Adjoint-Based Optimization for Aeroacoustics Control. *AIAA J.* AIAA 2010-3818 .

Kuruvila, G., Ta, S. & Salas, M.D. 1994 Airfoil optimization by the one-shot method. *Tech. Rep.*.

Lodato, Guido, Domingo, Pascale & Vervisch, Luc 2008 Three-dimensional boundary conditions for direct and large-eddy simulation of compressible viscous flows. *Journal of Computational Physics* **227** (10), 5105 – 5143.

Mani, A. 2012 Analysis and optimization of numerical sponge layers as a nonreflective boundary treatment. *J. Comput. Physics* **231**, 704–716.

Marinc, Daniel & Foysi, Holger 2012 Investigation of a continuous adjoint-based optimization procedure for aeroacoustic control of plane jets. *International Journal of Heat and Fluid Flow* **38** (0), 200 – 212.

Marschner, A.R. & Lobb, R. J. 1994 An evaluation of reconstruction filters for volume rendering. *In Proceedings of the conference on Visualization94, IEEE Computer Society Press.* pp. 100–107.

Mathew, J., Foysi, H. & Friedrich, R. 2006 A new approach to LES based on explicit filtering. *Int. J. Heat Fluid Flow* **27(4)**, 594–602.

Mathew, J., Lechner, R., Foysi, H., Sesterhenn, J. & Friedrich, R. 2003 An explicit filtering method for large eddy simulation of compressible flows. *Phys. Fluids* **15(8)**, 2279–2289.

Nocedal, J. & Wright, S. 2006 *Numerical Optimization*. Springer.

Rumpfkeil, Markus P. & Zingg, David W. 2010 A hybrid algorithm for far-field noise minimization. *Computers & Fluids* **39** (9), 1516 – 1528.

Spagnoli, B. & Airiau, C. 2008 Adjoint analysis for noise control in a two-dimensional compressible mixing layer. *Computers & Fluids* **37** (4), 475 – 486, turbulent Flow and Noise Generation.

Srinath, D.N. & Mittal, Sanjay 2010 An adjoint method for shape optimization in unsteady viscous flows. *Journal of Computational Physics* **229** (6), 1994 – 2008.

Stanley, S.A. & Sarkar, S. 2000 Influence of Nozzle Conditions and Discrete Forcing on Turbulent Planar Jets. *AIAA* **38**, 1615–1623.

Stolz, S. & Adams, N.A. 1999 An approximate deconvolution procedure for large-eddy simulation. *Phys. Fluids* **11**, 1699–1701.

Stolz, S., Adams, N. A. & Kleiser, L. 2001 An approximate deconvolution model applied for large-eddy simulation with application to incompressible wall-bounded flows. *Phys. Fluids* **13**, 997–.

Wei, M. & Freund, J. B. 2006 A noise-controlled free shear flow. *Journal of Fluid Mechanics* **546**, 123–152.

Zymaris, A.S., Papadimitriou, D.I., Giannakoglou, K.C. & Othmer, C. 2010 Adjoint wall functions: A new concept for use in aerodynamic shape optimization. *J.Comput. Physics* **229** (13), 5228 – 5245.